

Coupling erbium spins to a three-dimensional superconducting cavity at zero magnetic field

Yu-Hui Chen,* Xavier Fernandez-Gonzalvo, and Jevon J. Longdell†

*The Dodd-Walls Centre for Photonic and Quantum Technologies & Department of Physics,
University of Otago, 730 Cumberland Street, Dunedin, New Zealand.*

(Dated: December 8, 2024)

We experimentally demonstrate the coupling of an erbium doped crystal to a three-dimensional superconducting cavity of a 10^5 Q -factor at zero magnetic field. A tunable loop-gap resonator is used to match the cavity frequency to the hyperfine transitions of an erbium sample. The observed spectrum differs from what predicted by the published spin Hamiltonian parameters. The narrow cavity linewidth also enables the observations of asymmetric lineshapes of these hyperfine transitions, which are understood as the super-hyperfine interactions between the erbium ions and their adjacent yttrium ions. Such a broadly tunable superconducting cavity architecture, from 1.6 GHz to 4.0 GHz in the current design, is promising in building hybrid quantum systems.

PACS numbers: 32.10.Fn, 31.30.Gs, 42.50.Pq, 32.70.Jz

A quantum information system relies on the performances of the transfer, storage and processing of quantum states. Diverse platforms, such as atoms¹, photons², and macroscopic superconducting qubits³, have shown their own advantages in building sub-systems of a full quantum network. To combine the best features of these parts, such as the long coherence time of atoms, the ability of telecom photons to send quantum states over long distances, and the flexibility of superconducting qubits, hybrid quantum systems are proposed to be a promising direction⁴⁵. One important physical realization is to couple atomic spins to a microwave cavity⁶⁷⁸, where the electromagnetic field acts as a readout and the spins can either be used to store or process quantum informations. Cavity quantum electrodynamics (QED) provides the basic framework to reach this goal.

Due to the unique optical transition in $1.5 \mu\text{m}$ and the long optical coherence time⁹, erbium-doped crystals have attracted considerable interest from the field of hybrid quantum system. Recently erbium-doped crystals are proposed to be used in quantum conversions between microwave photons and optical photons¹⁰¹¹. The first step towards this goal, i.e., the coherent conversion from microwave to optical signals, is soon experimentally demonstrated¹². In addition erbium 167 atoms with non zero nuclear spins have rich hyperfine structures at zero magnetic field, and the prospect of using their nuclear spins to store quantum states¹³, is attractive. These merits have made erbium atoms an excellent candidate for hybrid quantum systems.

To date, encouraging results of the cavity QED of erbium spins (Er) coupled to various cavities have been obtained in experiments⁸¹⁴¹⁵¹⁶¹⁷. Strong couplings have been demonstrated in two-dimensional coplanar superconducting cavities⁸¹⁴ and three-dimensional (3D) copper cavities¹⁵¹⁶. These reported results are based on magnetically tuning spin transitions to match a fixed cavity frequency. In this paper we present the experimental results of an isotope-167-pure erbium ions ($^{167}\text{Er}^{3+}$) doped yttrium orthosilicate (Y_2SiO_5) crys-

tal coupled to a 3D superconducting cavity at zero magnetic field. A tunable loop-gap cavity is employed to drag the cavity frequency to the zero field transitions of $^{167}\text{Er}^{3+}$, which then gives out detectable zero-field electron-paramagnetic-resonance (EPR) signals. A high Q -factor of cavity, a controllable environment to reduce the decoherence effects, and a narrow inhomogeneous linewidth are desired for most cavity QED systems. Compared to other systems Our approach shows advantages in all these three aspects. First of all, because the superconductivity is not deteriorated by the applied magnetic field¹⁸, and at the same time the dielectric loss of the crystal doesn't add to the system due to the position of the sample is in the minimum of cavity electric field, our cavity works at $Q \sim 10^5$ and gives out higher sensitivity that enables us to see even finer structures. Nowadays typical 3D accelerator cavities and Fabry-Pérot cavities¹⁹ have Q -factors of 10^{10} , which correspond to a coherence time of 1 s. Our proposed is compatible with these available superconducting techniques and therefore holds the potential of greatly enhancing the light-matter interaction. Secondly, a 3D cavity enables a controllable coupling of qubits to the environment to reduce the decoherence²⁰²¹ and even the engineering of the quantum bath seen by the embedded qubits²². Besides, narrow inhomogeneous linewidths are expected in our approach not only because the absence of an imperfect magnetic field but also the magnetic inequivalence of atoms vanish²³.

Our experimental setup is shown in Fig. 1(a). The loop-gap resonator is made from niobium with an erbium sample sitting in its central hole. The used sample is a cylindrical Y_2SiO_5 crystal doped with $^{167}\text{Er}^{3+}$ ions at number concentration of 0.005% (Scientific Materials Inc). The sample is 4.95 mm in diameter and 12 mm in length. Y_2SiO_5 has three orthogonal optical extinction axes \mathbf{D}_1 , \mathbf{D}_2 , and \mathbf{b} . The \mathbf{b} axis of the crystal is aligned along the long axis of the cylinder, and the \mathbf{D}_1 - \mathbf{D}_2 plane is parallel to the end faces. The sample is mounted in the central hole with \mathbf{D}_1 perpendicular to the gap, as

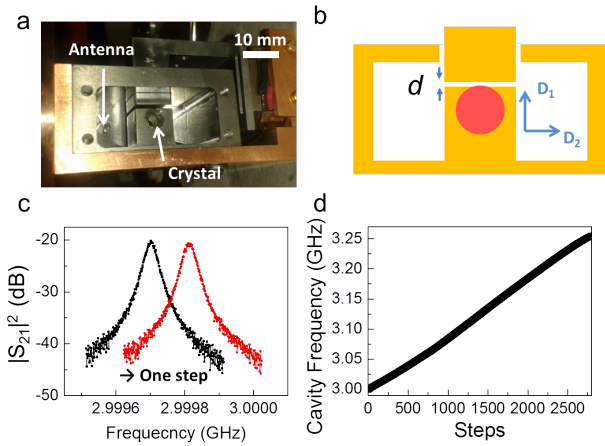


FIG. 1: (a) Photo of the loop-gap cavity. A $^{167}\text{Er}^{3+}$ doped Y_2SiO_5 sits in the central hole. Two short straight wires are inserted into the cavity to serve as antennae. A separated plunger is able to move up and down to change the gap size. Scale bar is 10 mm. (b) Schematic of our tunable loop-gap resonator. The cavity frequency can be shifted by changing the gap size d . The optical axes of Y_2SiO_5 are oriented as noted. (c) Typical cavity transmission curves. Shown are two $|S_{21}|^2$ curves recorded at two steps of the piezoceramic. Typical linewidth of the cavity is 30 kHz (d) Frequency tunability of the cavity. The peak positions of the transmission curves are recognized as the cavity resonant frequencies. As the gap size is moved step by step, the cavity frequency increases.

illustrated in Fig 1(b). Y_2SiO_5 is a monoclinic structure with two inequivalent sites (site 1 and site 2) where $^{167}\text{Er}^{3+}$ irons can substitute to yttrium irons. If the external static magnetic field is not aligned along the \mathbf{b} axis or the \mathbf{D}_1 - \mathbf{D}_2 plane, it is expected to see two magnetically inequivalent subclasses for each site²⁴. The ground state of erbium $^4I_{15/2}$ is split into eight levels by the crystal field of Y_2SiO_5 with only the lowest level is populated at cryogenic temperature. Our cavity with sample embedded is cooled down to 5.1 K (measured in the body of the cavity) by the use of a vibration isolated cryostat (Cold head: Cryomech PT405). Because $^{167}\text{Er}^{3+}$ irons have nuclear spin $I = 7/2$ and an effective electronic spin $S = 1/2$, the lowest crystal field level is then split into 16 hyperfine levels even in the absence of any ambient magnetic field. These hyperfine splittings can be understood from the spin Hamiltonian^{25,26}

$$H = \beta_e \mathbf{B} \cdot \mathbf{g} \cdot \mathbf{S} + \mathbf{S} \cdot \mathbf{A} \cdot \mathbf{I} + \mathbf{I} \cdot \mathbf{Q} \cdot \mathbf{I} \quad (1)$$

where β_e is the electronic Bohr magneton, \mathbf{B} the static magnetic field, \mathbf{g} the g-matrix of Zeeman effect, \mathbf{A} the hyperfine matrix, and \mathbf{Q} the electric quadrupole matrix. At 5.1 K all these 16 levels are populated and there are 120 possible transitions between them. Matching the cavity frequency to one of these transitions may give out a detectable zero-field EPR signal²³.

The design of our tunable cavity is based on a typical three-loop, two-gap configuration²⁷. The gaps here act

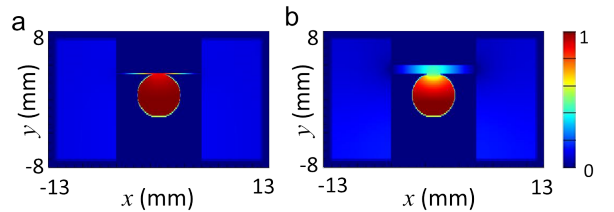


FIG. 2: Field distributions of the tunable loop-gap resonator. (a) 0.1 mm gap, corresponding to a cavity resonant frequency of 2.51 GHz. (b) 1 mm gap, cavity frequency 5.27 GHz. Shown in the figures are the magnitude of oscillating magnetic field, i.e., $|B|$, which are normalized to their individual maxima. Simulations are carried out on FDTD Solutions, Lumerical Solutions, Inc.

as capacitors while the loops act as inductors; the cavity resonance can be modelled as an LC circuit. Shown in Fig. 1(b) is a schematic of this tunable cavity. A plunger is separated from the main part of the cavity. By moving the plunger up and down one can change the gap d , which alters the capacitors and therefore the resonant cavity frequency. In our experiment the plunger is installed on a piezoelectric actuator, and one typical step of the actuator is 30 nm which corresponds to 0.1 MHz frequency shift. The set-up shown in Fig.1(a) has a tunable range from 1.6 GHz to 4.0 GHz. To minimize the energy radiated out from the cavity, two caps are added on both ends. Two short straight wires serving as coupling antennae are inserted into the cavity through two 5-mm-diameter windows on these two caps (Fig. 1(a)). The two antennae are connected to a network analyser and the transmission signal S_{21} is measured. By scanning the input microwave frequency, one can see a transmission peak once the input frequency meets the cavity resonant frequency, as shown in the left black curve in Fig. 1(c). Using an actuator to move the plunger one step outwards, we observed that the cavity frequency is increased approximately 0.1 MHz, as shown in the right red curve in Fig. 1(c). Note that attenuators and amplifiers are used in room temperature and their contributions (but not the signal losses caused by wires) in $|S_{21}|^2$ are already subtracted in the figures shown in this paper. Figure 1(d) confirms the tunability of our cavity. As the plunger is moved step by step, the cavity resonant frequency goes up almost linearly. As shown in Fig. 1(c) our cavity has a typical linewidth of 30 kHz at those off resonance frequencies, i.e., $Q \approx 9 \times 10^4$. This linewidth is not the intrinsic linewidth of our system but limited by the vibration of the cryostat. In the experiment the $\omega_c/2\pi$ is scanned around 3 GHz, whose gap size is approximately 0.5 mm; the gap merely need to be changed 0.3 nm in order to introduce a 1 kHz shift to $\omega_c/2\pi$ ²⁷. Therefore small vibrations do affect our detections. at the instant when switching the cryostat off (still cold and no vibrations), $Q \approx 20 \times 10^4$ were observed at off resonance frequencies.

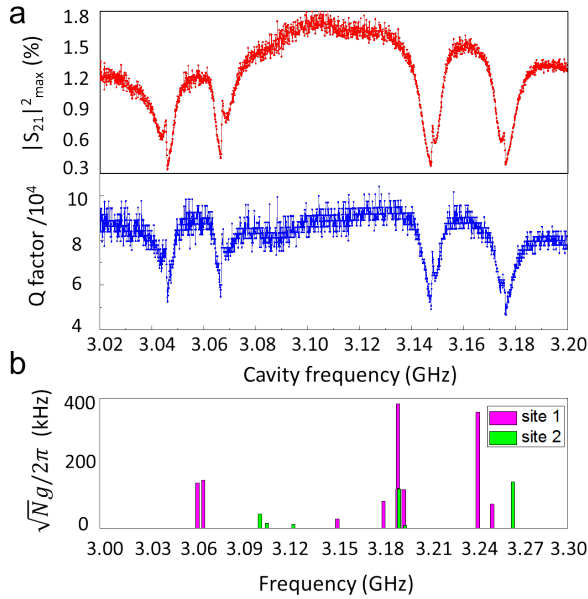


FIG. 3: (a) Experimental results of zero-field EPR. The transmission $|S_{21}|^2$ at cavity resonant frequencies ν and the Q factors are measured when the cavity frequency moves. Top, transmission as a function of cavity frequency. Down, Q -factor as a function of cavity frequency. The transmission signals are shown in linear scale. The cavity frequency is moved approximately 0.1 MHz per step. (b) Calculated collective coupling strengths of $^{167}\text{Er}:\text{YSO}$ at around 3.1 GHz at zero magnetic field. Pink bar, transitions of site 1; green bar, transitions of site 2.

Besides the good filling factor¹⁰, another outstanding feature of this tunable loop-gap cavity is that the field distribution in the central hole stays uniform during the cavity frequency tuning. Shown in Fig. 2 are simulated field distributions for two different gap widths. They are cross sections in the middle of the cavity when viewed along the long axis of the crystal. When the gap $d = 0.1\text{mm}$, the cavity frequency is 2.51 GHz. It is clear that most energy is confined uniformly in the central hole where sits our sample. When the gap is increased to $d = 1\text{mm}$, the frequency goes up to 5.27 GHz. The field distribution is still uniform though some field leaks from the central hole. In our zero-field EPR experiment the frequency range is from 3.02 GHz to 3.20 GHz, where the field distribution is considered to be the same.

Figure 3(a) shows our experimental results by scanning the cavity from 3.02 GHz to 3.20 GHz. In all steps of the actuator we used the network analyser to measure the frequency-dependent transmission curves. Those frequencies where transmission curves have their maxima $|S_{21}|^2_{\text{max}}$ are considered as cavity frequencies. When the cavity frequency $\omega_c/2\pi$ is tuned into resonance with one of those hyperfine spin transitions, a decrease in the transmission is expected due to the coupling between the cavity mode and the spin ensemble. In the weak cou-

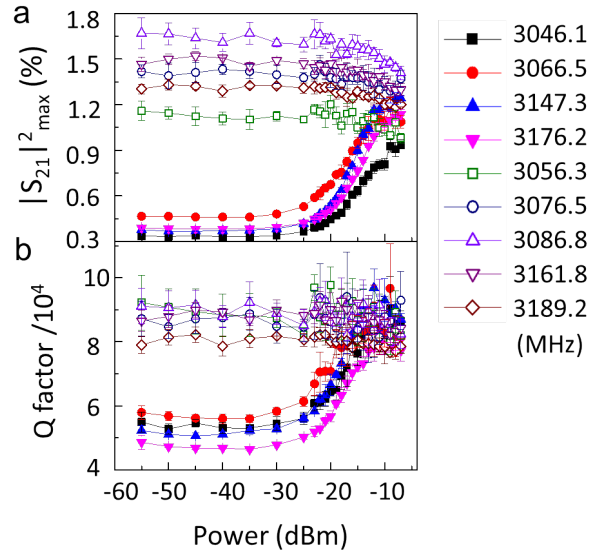


FIG. 4: Saturations of erbium atoms at high power inputs. (a) Peak transmission as a function of input power at several cavity frequencies as noted. (b) Q -factor as a function of input power at several frequencies as noted. Here the input power is defined as the power immediately after the attenuators. Those four solid-filled-symbol curves in each figure correspond to the four dips in Fig. 3, while the other empty-symbol curves are randomly chosen from off-resonant positions.

pling regime the spin ensemble provides an additional loss channel for the cavity field and therefore both $|S_{21}|^2_{\text{max}}$ and the Q -factor drops in those resonant frequencies, as shown in Fig. 3(a). Note that the effect of the erbium ions pulling the cavity frequency when close to resonances is neglected, because the resulting frequency shifts in our experiments are on the order of 1 kHz. Four transition minima are identified in Fig. 3(a), which are 3045.946 MHz, 3066.458 MHz, 3147.368 MHz, and 3176.170 MHz, respectively.

To further confirm these zero-field EPR signals come from the erbium atoms, saturation effects under high power inputs at nine different cavity frequencies are shown in Fig. 4. Four of them correspond to the four minima in Fig. 3(a) and the other five are randomly-chosen off-resonant frequencies. For each curve $|S_{21}|^2_{\text{max}}$ and the corresponding Q -factor are measured as a function of the input power. For those off-resonant frequencies the responses of $|S_{21}|^2_{\text{max}}$ and Q factor shows no input dependence, as shown by the empty-symbol curves in Fig. 4. (the slightly declinings are originated from the power dependence of superconductivity¹⁸). If $\omega_c/2\pi$ is tuned to match the spin transitions, the input microwave is absorbed and results in a low $|S_{21}|^2_{\text{max}}$ and a low Q factor. When the number of erbium atoms are not enough to absorb the same fraction of the input microwave, increases in both the transmission and the Q factor are expected, as shown in those solid-symbol curves in Fig. 4. The turning points for all the four dips are approximately at

-25 dBm, which corresponds to a total photon number inside the cavity of 5×10^{12} while the population difference of erbium spins of each magnetic site 1×10^{14} . The error bars in Fig. 4 again confirms that the background measurements are limited by vibrations. As the cavity linewidth is already broad, the vibration effects is less significant (error bars of solid-symbol curves in Fig. 4).

Based on Eq. (1) and the matrices in literature²⁶, the collective coupling strength $\sqrt{N}g$ of $^{167}\text{Er}:\text{YSO}$ coupled to our loop-gap resonator at zero magnetic field at the temperature of 5.1 K is calculated and shown in Fig. 3(b). In the calculation the effects of finite temperature are simply included by taking into account the Boltzmann factors. The deviations between our measurements and the predicted transition frequencies are at the order of several tens of MHz. This shows that the spin Hamiltonian determined at high magnetic field is imperfect when the results are extrapolated at zero magnetic field.

Because linewidth of the superconducting cavity is approximately 30 kHz, which is much less than the MHz inhomogeneous linewidths, we were able to see even finer structures of these hyperfine transitions. In Fig. 3(a) each minimum shows an asymmetric line-shape. Magnified views of $|S_{21}|_{\text{max}}^2$ and Q of the 3045.946 MHz data are shown in Fig. 5, with two shoulders and a sharp edge clearly identified. In our experiment there is no magnetic shield to shield the earth field (approximately 100 μT) from the niobium cavity²⁸. For two reasons those 1 MHz splittings can not be ascribed to the response of the two inequivalent magnetic sites of Er²⁴. First, no changes in the transition frequencies or the splittings were observed by rotating our sample and cavity; second, Er of two different magnetic sites are too far to interact with each other and can only produce two Lorentz-shape lines. These non Lorentz lineshapes indicate that the observed hyperfine transition involves even finer interactions. We attribute this to the superhyperfine interactions between Er ions and the closest yttrium (Y) ions^{29,30}. The Hamiltonian of an electron spin ensemble coupled to a cavity and their host nuclear spins can be written as

$$H_{sys} = \omega_c a^\dagger a + \sum_k \omega_{g,k} |g\rangle\langle g|_k + \omega_{e,k} |e\rangle\langle e|_k + \sum_k \mathcal{B}_k (a + a^\dagger) \mathbf{g} \mathbf{S}_k + \mathbf{S}_k \mathbf{\Lambda} \mathbf{I}_k \quad (2)$$

where where ω_c is the cavity frequency, a is the cavity annihilation operator, $\omega_{g,k}$ is the energy of the hyperfine ground state of the k th atom, $\omega_{e,k}$ is the energy of the excited state, $|g\rangle\langle g|_k$ and $|e\rangle\langle e|_k$ are the projection operators, \mathcal{B}_k is the electromagnetic field at the k th atom, \mathbf{S}_k is the electron spin of the k th Er ion, \mathbf{g} is the g-factor matrix for Er ions, and \mathbf{I}_k is the nuclear spin of the k th Y ion. The term of $\mathbf{S}_k \mathbf{\Lambda} \mathbf{I}_k$ stands for the anisotropic coupling interactions between Er and Y. H_{sys} can be diagonalized to give out four energy levels, among which two are allowed transitions and two are partially forbidden³⁰. If the linewidths of this system are determined by spontaneous emission, obtaining

the lineshapes of these two allowed transition is easy as the Lindblad loss operators are originated from two uncorrelated bath. However what is dominant in our experiment is the inhomogeneous effect, which means that the two allowed transitions coupled to the cavity mode share a same "inhomogeneous bath". A detailed analysis of the decoherence processes is complicated and over the scope of this paper. An intuitive way to try is including an additional interaction term between these two allowed transitions in the Hamiltonian and then assuming they have two uncorrelated bathes. Noting that for large atom-ensembles with few excitations the motions of collective atomic transitions can be approximated by bosonic modes^{31,32,33}, here we consider our system, phenomenologically, as a cavity interacts with two coupled atom-ensembles:

$$H_{model} = \omega_c a^\dagger a + \omega_1 b_1^\dagger b_1 + \omega_2 b_2^\dagger b_2 + \sqrt{N} g_1 (b_1^\dagger a + b_1 a^\dagger) + \sqrt{N} g_2 (b_2^\dagger a + b_2 a^\dagger) + \delta b_1^\dagger b_2 + \delta b_2^\dagger b_1 \quad (3)$$

where b_1 and b_2 are two commutated bosonic annihilation operators (the two allowed transitions) with frequencies ω_1 and ω_2 respectively, $\sqrt{N}g_1$ and $\sqrt{N}g_2$ are their collective coupling strengths to the cavity, and δ stands for the coupling between them. Here b_1 and b_2 coupled to two uncorrelated bathes characterized by linewidths Γ_1^* and Γ_2^* .

To fit the experiment data, we used the model above together with the cavity input-output theory³⁴ to calculate the spectrum response of our system, and then extracted the $|S_{21}|_{\text{max}}^2$ and Q for each cavity frequency ω_c . The fittings of the experimental data of 3045.946 MHz are plot as black curves in Fig. 5(a). Good agreements can be seen in both $|S_{21}|_{\text{max}}^2$ and Q . From the fittings we know that the coupling strengths of the spin ensemble for the 3045.946 MHz data are $\sqrt{N}g_1/2\pi = 37$ kHz and $\sqrt{N}g_2/2\pi = 145$ kHz, the linewidths are $\Gamma_1^*/2\pi = 450$ kHz and $\Gamma_2^*/2\pi = 6$ MHz, $(\omega_1 - \omega_2)/2\pi = -1$ MHz, and $\delta/2\pi = 700$ kHz. Worthy of noting is that $|\omega_1 - \omega_2|/2\pi$ and $\delta/2\pi$ used in those fittings are approximately 1 MHz, which agrees with the reported superhyperfine parameters of Er-Y interactions³⁰ and the coupling strengths being around 100 kHz agree with Fig. 3(b). As $\Gamma_1^* \ll \Gamma_2^*$, we characterize the observed lineshapes as Fano resonances³⁵, i.e., a narrow transition lies with in the inhomogeneous range of another broad transition and their interference gives out an asymmetric lineshape with a sharp edge. At 3045.946 MHz, the Fano resonance enhances the coupling of our cavity mode to the atomic transition b_1 and suppresses the coupling to b_2 .

Discussion: Among those four minima in Fig. 3(a), the strongest collective coupling strength observed in the above experiment happens in the 3147.3 MHz resonance with $\sqrt{N}g_2/2\pi = 185$ kHz and $\Gamma_2^*/2\pi = 5800$ MHz. Use the common criteria for strong coupling, our experiments has $Ng_2^2/\kappa\Gamma_2^* \approx 0.2$, with $\kappa/2\pi = 30$ kHz the cavity

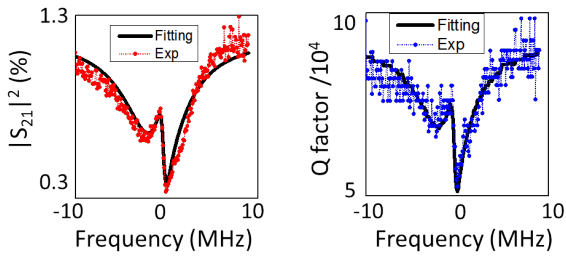


FIG. 5: Model for the experimental results. Fittings for the data of 3045.946 MHz. Above: black solid curve, fitting for $|S_{21}|^2$; red dot curve, experimental data. Below: black solid curve, fitting for Q ; red dot curve, experimental data. The two fittings are under the same set of parameters.

loss, which indicates that our system is not yet working in the strong coupling regime. A intuitive way toward the strong coupling is reducing the working temperature from the current 5.1 K to mK, which increases the collective number N dramatically and may at the same time minimizing the de-coherent effects. Once the spin Hamiltonian is determined precisely in zero magnetic field, we

may also benefit from looking for transitions of higher transition strengths. At the same time the shape edge of Fano lineshape may also be a positive factor. Achieving strong coupling for erbium ensembles at zero static magnetic field is challenging and promising.

In conclusion, we have demonstrated the coupling of an $^{167}\text{Er}:\text{YSO}$ crystal to a 3D superconducting cavity at zero magnetic field at 5.1 K. Four asymmetric line-shape resonances are characterized as Fano resonances of discrete states of sub-MHz linewidth embedded into 5 MHz linewidth continua, whose collective coupling strengths to the cavity mode are approximately 50 kHz and 150 kHz. This phenomenon is understood as the interactions of erbium ions and their adjacent yttrium ions. A tunable superconducting cavity architecture with a high Q -factors and zero magnetic field enables the observation of finer structures and the complicated manipulations of coherence processes, which show prospective implementation in spectroscopy and quantum information.

This work was sponsored by the Marsden Fund (Contract No. UOO1221) of the Royal Society of New Zealand.

* stephen.chen@otago.ac.nz

† jevon.longdell@otago.ac.nz

¹ E. Saglamyurek, J. Jin, V. B. Verma, M. D. Shaw, F. Marsili, S. W. Nam, D. Oblak, and W. Tittel, *Nat. Photonics* **9**, 83 (2015), ISSN 1749-4885, URL <http://www.nature.com/doi/10.1038/nphoton.2014.311>.

² A. Aspuru-Guzik and P. Walther, *Nat. Phys.* **8**, 285 (2012), ISSN 1745-2473, URL <http://www.nature.com/doi/10.1038/nphys2253>.

³ A. a. Houck, H. E. Türeci, and J. Koch, *Nat. Phys.* **8**, 292 (2012), ISSN 1745-2473, URL <http://www.nature.com/doi/10.1038/nphys2251>.

⁴ G. Kurizki, P. Bertet, Y. Kubo, K. Mølmer, D. Petrosyan, P. Rabl, and J. Schmiedmayer, *Proc. Natl. Acad. Sci. U. S. A.* **112**, 3866 (2015), ISSN 1091-6490, URL <http://www.ncbi.nlm.nih.gov/pubmed/25737558>.

⁵ Z.-L. Xiang, S. Ashhab, J. You, and F. Nori, *Rev. Mod. Phys.* **85**, 623 (2013), ISSN 0034-6861, URL <http://link.aps.org/doi/10.1103/RevModPhys.85.623>.

⁶ Y. Kubo, F. R. Ong, P. Bertet, D. Vion, V. Jacques, D. Zheng, a. Dréau, J.-F. Roch, a. Auffeves, F. Jelezko, et al., *Phys. Rev. Lett.* **105**, 140502 (2010), ISSN 0031-9007, URL <http://link.aps.org/doi/10.1103/PhysRevLett.105.140502>.

⁷ D. I. Schuster, a. P. Sears, E. Ginossar, L. DiCarlo, L. Frunzio, J. J. L. Morton, H. Wu, G. a. D. Briggs, B. B. Buckley, D. D. Awschalom, et al., *Phys. Rev. Lett.* **105**, 140501 (2010), ISSN 0031-9007, URL <http://link.aps.org/doi/10.1103/PhysRevLett.105.140501>.

⁸ S. Probst, H. Rotzinger, S. Wünsch, P. Jung, M. Jerger, M. Siegel, a. V. Ustinov, and P. a. Bushev, *Phys. Rev. Lett.* **110**, 157001 (2013), ISSN 0031-9007, URL <http://link.aps.org/doi/10.1103/PhysRevLett.110.157001>.

⁹ C. Thiel, T. Böttger, and R. Cone, *J. Lumin.* **131**,

353 (2011), ISSN 00222313, URL <http://linkinghub.elsevier.com/retrieve/pii/S002223131000534X>.

¹⁰ L. A. Williamson, Y.-H. Chen, and J. J. Longdell, *Phys. Rev. Lett.* **113**, 203601 (2014), ISSN 0031-9007, URL <http://link.aps.org/doi/10.1103/PhysRevLett.113.203601>.

¹¹ C. O'Brien, N. Lauk, S. Blum, G. Morigi, and M. Fleischhauer, *Phys. Rev. Lett.* **113**, 063603 (2014), ISSN 0031-9007, URL <http://link.aps.org/doi/10.1103/PhysRevLett.113.063603>.

¹² X. Fernandez-gonzalvo, Y.-h. Chen, C. Yin, S. Rogge, and J. J. Longdell, pp. 1–6 (2015).

¹³ G. Wolfowicz, H. Maier-Flaig, R. Marino, A. Ferrier, H. Vezin, J. J. L. Morton, and P. Goldner, **1**, 5 (2014), 1412.7298, URL <http://arxiv.org/abs/1412.7298>.

¹⁴ A. Tkalčec, S. Probst, D. Rieger, H. Rotzinger, S. Wünsch, N. Kukharchyk, a. D. Wieck, M. Siegel, a. V. Ustinov, and P. Bushev, *Phys. Rev. B* **90**, 075112 (2014), ISSN 1098-0121, URL <http://link.aps.org/doi/10.1103/PhysRevB.90.075112>.

¹⁵ S. Probst, A. Tkalčec, H. Rotzinger, D. Rieger, J.-M. Le Floch, M. Goryachev, M. E. Tobar, A. V. Ustinov, and P. A. Bushev, *Phys. Rev. B* **90**, 100404 (2014), ISSN 1098-0121, URL <http://link.aps.org/doi/10.1103/PhysRevB.90.100404>.

¹⁶ P. A. B. S. Probst, H. Rotzinger, A. V. Ustinov, p. 12 (2015), 1501.01499, URL <http://arxiv.org/abs/1501.01499>.

¹⁷ S. Probst, N. Kukharchyk, H. Rotzinger, a. Tkalčec, S. Wünsch, a. D. Wieck, M. Siegel, a. V. Ustinov, and P. a. Bushev, *Appl. Phys. Lett.* **105**, 162404 (2014), ISSN 0031-9007, URL <http://scitation.aip.org/content/aip/journal/apl/105/16/10.1063/1.4898696>.

¹⁸ S. E. D. Graaf, a. V. Danilov, a. Adamyan, T. Bauch, and

- S. E. Kubatkin, *J. Appl. Phys.* **112**, 123905 (2012), ISSN 00218979, URL <http://scitation.aip.org/content/aip/journal/jap/112/12/10.1063/1.4769208>.
- ¹⁹ S. Kuhr, S. Gleyzes, C. Guerlin, J. Bernu, U. B. Hoff, S. Deleglise, S. Osnaghi, M. Brune, J.-M. Raimond, S. Haroche, et al., *Appl. Phys. Lett.* **90**, 164101 (2007), ISSN 00036951, URL <http://scitation.aip.org/content/aip/journal/apl/90/16/10.1063/1.2724816>.
- ²⁰ H. Paik, D. I. Schuster, L. S. Bishop, G. Kirchmair, G. Catelani, a. P. Sears, B. R. Johnson, M. J. Reagor, L. Frunzio, L. I. Glazman, et al., *Phys. Rev. Lett.* **107**, 240501 (2011), ISSN 0031-9007, URL <http://link.aps.org/doi/10.1103/PhysRevLett.107.240501>.
- ²¹ C. Rigetti, J. M. Gambetta, S. Poletto, B. L. T. Plourde, J. M. Chow, a. D. Córcoles, J. a. Smolin, S. T. Merkel, J. R. Rozen, G. a. Keefe, et al., *Phys. Rev. B* **86**, 100506 (2012), ISSN 1098-0121, URL <http://link.aps.org/doi/10.1103/PhysRevB.86.100506>.
- ²² K. W. Murch, S. J. Weber, K. M. Beck, E. Ginossar, and I. Siddiqi, *Nature* **499**, 62 (2013), ISSN 1476-4687, URL <http://www.ncbi.nlm.nih.gov/pubmed/23823794>.
- ²³ R. Bramley and S. J. Strach, pp. 49–82 (1983).
- ²⁴ Y. Sun, T. Böttger, C. Thiel, and R. Cone, *Phys. Rev. B* **77**, 085124 (2008), ISSN 1098-0121, URL <http://link.aps.org/doi/10.1103/PhysRevB.77.085124>.
- ²⁵ H. Search, C. Journals, A. Contact, M. Iopscience, and I. P. Address, **25** (????).
- ²⁶ O. Guillot-Noël, P. Goldner, Y. Du, E. Baldit, P. Monnier, and K. Bencheikh, *Phys. Rev. B* **74**, 214409 (2006), ISSN 1098-0121, URL <http://link.aps.org/doi/10.1103/PhysRevB.74.214409>.
- ²⁷ R. L. Wood, W. Froncisz, and J. S. Hyde, *J. Magn. Reson.* **58**, 243 (1984), ISSN 00222364, URL <http://linkinghub.elsevier.com/retrieve/pii/0022236484902142>.
- ²⁸ S. Aull, O. Kugeler, and J. Knobloch, *Phys. Rev. Spec. Top. - Accel. Beams* **15**, 062001 (2012), ISSN 1098-4402, URL <http://link.aps.org/doi/10.1103/PhysRevSTAB.15.062001>.
- ²⁹ L. Rowan, E. Hahn, and W. Mims, *Phys. Rev.* **137**, A61 (1965), ISSN 0031-899X.
- ³⁰ O. Guillot-Noël, H. Vezin, P. Goldner, F. Beaudoux, J. Vincent, J. Lejay, and I. Lorgeré, *Phys. Rev. B* **76**, 180408 (2007), ISSN 1098-0121, URL <http://link.aps.org/doi/10.1103/PhysRevB.76.180408>.
- ³¹ T. Holstein and H. Primakoff, *Phys. Rev.* **15**, 1098 (1940).
- ³² R. H. Dicke, *Physical Rev.* **24**, 99 (1953).
- ³³ I. Diniz, S. Portolan, R. Ferreira, J. M. Gérard, P. Bertet, and a. Auffèves, *Phys. Rev. A* **84**, 063810 (2011), ISSN 1050-2947, URL <http://link.aps.org/doi/10.1103/PhysRevA.84.063810>.
- ³⁴ C. W. Gardiner and P. Zoller, *Quantum noise* (Springer, 2000), 2nd ed.
- ³⁵ U. Fano, *Phys. Rev.* **124**, 1866 (1961).